

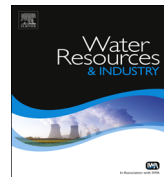


ELSEVIER

Contents lists available at ScienceDirect

Water Resources and Industry

journal homepage: www.elsevier.com/locate/wri



Highly efficient removal of basic blue 41 with nanoporous silica



Mansoureh Zarezadeh-Mehrizi*, Alireza Badiei*

School of Chemistry, College of Science, University of Tehran, Tehran, Iran

ARTICLE INFO

Article history:

Received 12 August 2013

Received in revised form

14 April 2014

Accepted 22 April 2014

Keywords:

Nanoporous silica

Waste water

Ethyl silicate

Cationic dye

Basic blue 41

ABSTRACT

The adsorption characteristics of basic blue 41 from aqueous solution were investigated using nanoporous silica (NPS). NPS with an average pore diameter of 2.4 nm and a surface area of 1030 m²/g was synthesized by using nonyl phenol ethoxylated decylether (NP-10) as structure directing agent (SDA) and ethyl silicate 40% (ETS-40) under acidic condition. This adsorbent was analyzed by means of small-angle X-ray scattering, scanning electron microscopy, N₂ adsorption–desorption isotherm and Fourier transforms infrared spectroscopy. The kinetic data reveals that the adsorption process follows the linear form of the pseudo-second-order model. The adsorption isotherm was fitted well to the Langmuir data. The monolayer adsorption capacity of adsorbent was found to be 345 mg/g.

© 2014 Published by Elsevier B.V. This is an open access article under the CC BY-NC-ND license

(<http://creativecommons.org/licenses/by-nc-nd/3.0/>).

1. Introduction

Synthetic dyes are widely used in different industries such as textile, leather, cosmetics, plastics, and food, annually [1]. Colored effluents of these industries not only have a negative effect on the aquatic system because of the blocking sunlight for photosynthesis process but also can be identified as the toxic and carcinogenic materials [2]. Azo dyes are the most common group of dyes used in textile industries because of their low cost, stability and variety of colors [3]. They are biologically non-degradable because of their aromatic structure, thereby, removal of these dyes are very important in

* Corresponding author. Tel.: +982161112614; fax: +982166495291.

E-mail addresses: mansourezare@gmail.com (M. Zarezadeh-Mehrizi), abadiei@khayam.ut.ac.ir (A. Badiei).

view point of the ecosystem and restriction on the water availability. There are various methods to remove dyes such as coagulation/flocculation, biological treatment, chemical oxidation, photocatalysis, membrane filtration, liquid–liquid extraction and adsorption [4–13]. Among these methods, adsorption has a good reliability for the industries due to easy operation, cost-effectiveness, high efficiency and water reuse. Different kinds of adsorbent are used for the removal of synthetic dyes such as activated carbons, zeolite, fly ash, graphene oxide and nanoporous silica [14–20]. Nanoporous silicas have attracted increasing attention because of high surface area and pore volume, adjustable pore diameter, their simple synthesis, high thermal and hydrothermal stability. Among different kinds of nanoporous silica, the family of MSU-X has a wormhole-like pore structure which facilitates the diffusion of reacting species to the reactive site. Despite this characteristic of MSU-X, there are a few studies that MSU-X materials are used as the adsorbent. Nanoporous silica and functionalized nanoporous silica have been used for dyes removal [9,21–23]. Research on the dye adsorption is limited to a few kinds of dyes such as methylene blue, phenosafranine and night blue [9,14,15,18,19,24–30] but there are a few reports about the adsorption of basic blue 41 [31–33].

In this study, NPS was prepared using NP-10 as a SDA and ETS-40 as a silica source in acidic media. The surfactants were removed from the framework by ethanol extraction and followed heating at 350 °C. The synthesized NPS used for the adsorption of basic blue 41, water-soluble cationic dye, as it is widely used in the textile industry. The adsorption behavior was evaluated by kinetic and isotherm studies.

2. Experimental

2.1. Materials

The chemicals used for the synthesis: ethyl silicate solution (ETS-40, Wacker, SiO₂ 40%), nitric acid (Merck, 65%), nonyl phenol ethoxylated decylether (Hulls, NP-10, M_w=660 g/mol), basic blue 41 (Ciba, M_w=452.58 g/mol, hereafter designated as BB 41), Ethanol and dionized water. Fig. 1 shows the chemical structure of BB 41.

2.2. Synthesis of nanoporous silica (NPS)

NPS was prepared as reported previously, using NP-10 as a SDA and ETS-40 as a silica source under acidic conditions [34]. Briefly, surfactant was dissolved in an acidic solution under stirring at 30 °C. Then, 196 g of ETS-40 was added to this solution and it was kept at 80 °C under stirring at 400 rpm during 5 h. the final composition is 1 SiO₂, 0.06 NP-10, 3.9 HNO₃ and 110 H₂O. The solid product was filtered, washed with deionized water and dried. Finally, the white solid was recovered after ethanol extraction with a Soxhlet apparatus and a further heating at 350 °C in air.

2.3. Batch adsorption experiment

Dye adsorption experiments onto NPS were performed by mixing 20 ml of BB 41 solution of desired initial concentration with 0.01 g of NPS at 30 °C. The pH of the solution was adjusted to 7 using dilute NaOH solution. Isotherm experiments were carried out at initial dye concentration from 48 to 360 mg/L. BB 41 adsorption kinetics over NPS were evaluated at different concentrations (20–60 mg/L) at predetermined time intervals between 5 and 180 min. The solid and liquid phases were separated

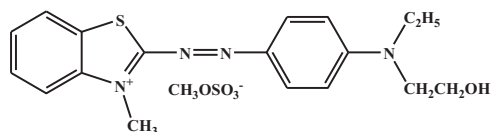


Fig. 1. Chemical structure of BB 41.

after equilibrium and the adsorbed amount of dye was calculated by Beer's law based on the absorption peak at 609 nm for BB 41.

The equilibrium adsorption capacity was determined according to the mass balance equation:

$$q_e = \frac{(C_0 - C_e)V}{m} \quad (1)$$

where C_0 is the initial dye concentration in the liquid phase (mg/L), C_e is the equilibrium concentration of dye (mg/L), V is the volume of dye solution used (L) and m is the mass of the adsorbent used (g).

2.4. Characterization

Scanning electron microscopy (SEM) observation was performed by Oxford LEO 1445 V. Nitrogen adsorption–desorption isotherm was measured at 70 K using a BELSORP-miniII. Prior to measurement, the nanoporous silica degassed at 573 K for 3 h. The Barrett–Emmett–Teller (BET) method was utilized to calculate the specific surface areas from the linear part of the BET plot over the relative pressure (p/p_0) range of 0.05–0.35; the pore size distribution was analyzed with the supplied BJH software package from the adsorption branches of the isotherm. The pore volume was taken at the $p/p_0=0.990$ point. The small-angle X-ray scattering (SAXS) pattern was collected in a range angle from 0 to 10° on a Hecus S3-MICRO_{pix} using Cu K α radiation. FT-IR spectra were obtained on Equinox 55 BRUKER model infrared spectrophotometer. Dye concentration change was recorded by a UV–vis spectrophotometer model Raylight UV-1600.

3. Results and discussion

3.1. Characterization of the NPS

Fig. 2a shows the SAXS pattern of the NPS obtained after the removal of surfactant. This pattern is very similar to MSU compound possessing nonordered wormlike pore structures with no long range order symmetry. They have one broad peak at about $2\theta=2^\circ$ corresponding to d_{100} reflections, assigned to the pore center-to-pore center correlation reflection.

The N₂ adsorption–desorption data presented in Fig. 2b is characteristic type IV isotherm and no apparent hysteresis loop is observed. The adsorption achieves saturation at a relative pressure about 0.3 which indicates the presence of mesopore channels (Fig. 2b). The textural properties of NPS are summarized in Fig. 2b (inset).

The morphology of NPS particles was examined by SEM observation. Fig. 3 reveals the agglomerated particles of several micrometers with rough surface.

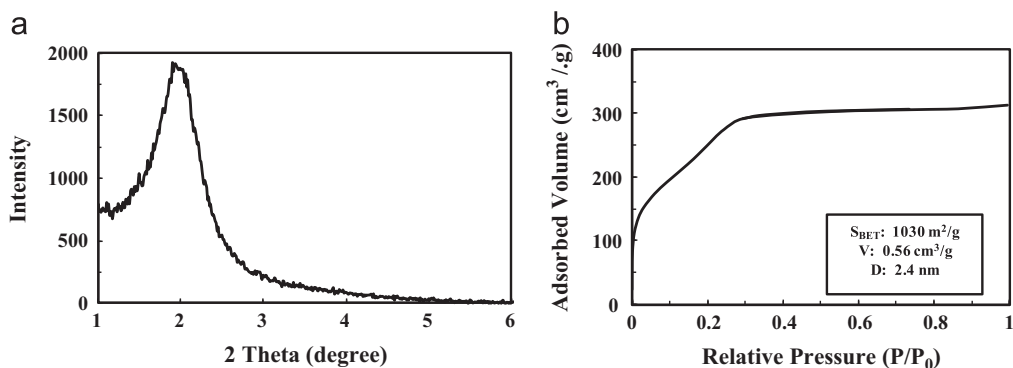


Fig. 2. (a) SAXS pattern of NPS after the removal of surfactant and (b) N₂ adsorption–desorption isotherm of NPS.

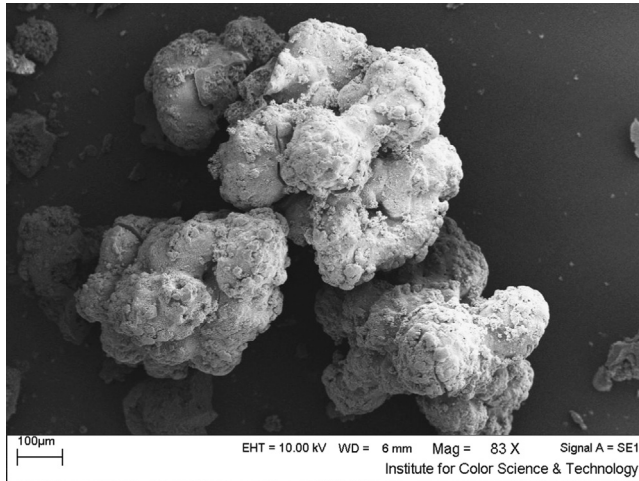


Fig. 3. SEM image of NPS.

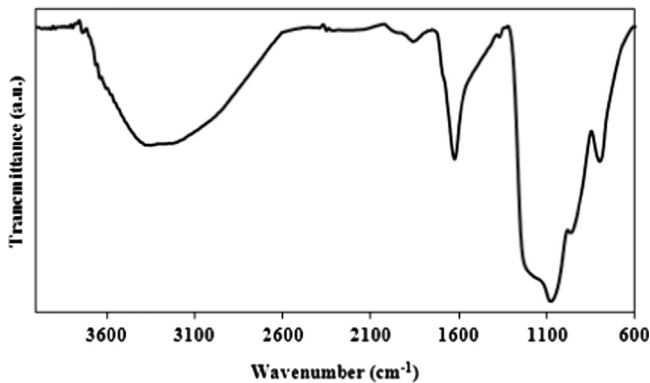


Fig. 4. FT-IR spectrum of NPS after the removal of surfactant.

The FT-IR spectrum of NPS is shown in Fig. 4. It can be found that the surfactant was removed completely. The broad band at 3400 cm^{-1} is attributed to O–H bond stretching vibration of adsorbed water molecules. This broad band exhibits the large amounts adsorption of water due to high contents of surface hydroxyl groups. NPS can be used as the adsorbent of water-soluble cationic azo dyes because of the high adsorption capacity for water. The strong peak at 1630 cm^{-1} is due to the bending vibrations of the corresponding stretching vibration mode. The peaks at 816 and 1100 cm^{-1} are assigned to the stretching vibration of Si–O–Si bonds of condensed silica network.

3.2. Dye adsorption

3.2.1. Adsorption equilibrium and kinetic analysis

The equilibrium study of the adsorption of BB41 onto NPS was performed with a different initial dye concentrations solution ($20\text{--}60\text{ mg/L}$). It is clearly observed from Fig. 5 that the steady state is reached within 60 min which denotes fast adsorption kinetics of the dye onto NPS.

The pseudo-first-order and pseudo-second-order models were applied to understand the detailed characteristics of the kinetic process.

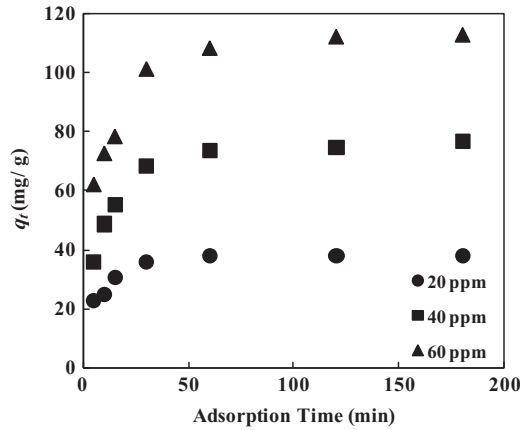


Fig. 5. Equilibrium studies of BB 41 adsorption onto NPS at different initial dye concentrations.

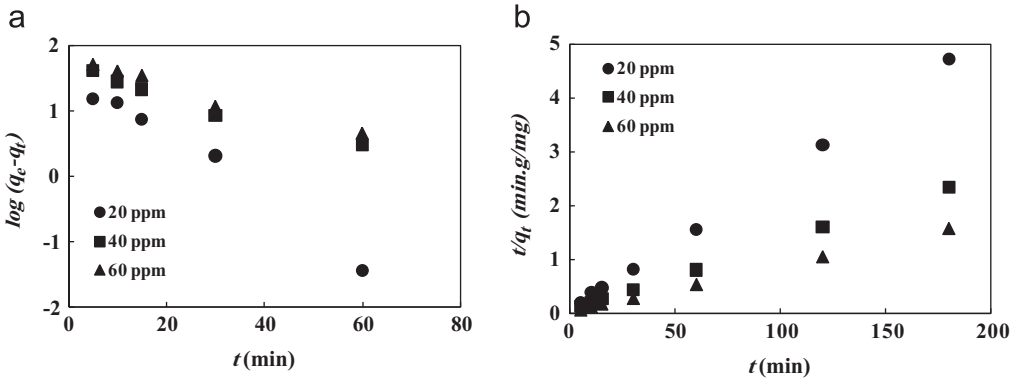


Fig. 6. (a) Pseudo-first-order and (b) pseudo-second-order kinetics for the adsorption of BB 41 onto NPS.

The pseudo-first-order model is expressed as a linear form equation:

$$\log(q_e - q_t) = \log q_e - \frac{k_1 t}{2.303} \quad (2)$$

where k_1 is the pseudo-first-order rate constant, q_e and q_t are the adsorption capacity of BB 41 onto the adsorbent at steady state and time t , respectively.

The linear form of pseudo-second-order kinetic model is expressed as follows:

$$\frac{t}{q_t} = \frac{1}{k_2 q_e^2} + \frac{t}{q_e} \quad (3)$$

where k_2 is the pseudo-second-order adsorption rate constant. The plots of $\log(q_e - q_t)$ versus time t based on pseudo-first-order kinetics and t/q_t versus t based on pseudo-second-order kinetics are compared in Fig. 6 (a and b), respectively. The fitting parameters of two kinetics model are listed in Table 1.

This finding suggests that the adsorption kinetics followed the pseudo-second-order model since this model gives greater correlation coefficient ($R^2 > 0.99$) than that of the first order. These results suggest that the adsorption process was controlled by chemisorption. The negative charged surface of NPS adsorbs the cationic dye molecules by the electrostatic attraction. The adsorption efficiencies were found to be more than 94% at the initial concentration of (20–60) mg/L.

Table 1

Kinetic parameters of the adsorption of BB 41 onto NPS obtained using pseudo-first-order and pseudo-second-order.

C_0 mg/g	$q_{e, \text{exp}}$ mg/g	Pseudo-first-order			Pseudo-second-order		
		k_1 min^{-1}	$q_{e, \text{cal}}$ mg/g	R^2	k_2 g/(mg. min)	$q_{e, \text{cal}}$ mg/g	R^2
20	38.12	0.112	37.61	0.9850	7.2×10^{-3}	39.37	0.9995
40	77.01	0.046	44.32	0.9764	2.1×10^{-3}	79.37	0.9998
60	113.264	0.045	61.29	0.9716	1.57×10^{-3}	117.65	0.9997

Considering that the pseudo-first-order and pseudo-second-order model could not identify the diffusion mechanism, the intraparticle diffusion model was taken into account. This model is expressed by

$$Q_t = k_i t^{1/2} + C \quad (4)$$

where k_i is the intraparticle diffusion constant and C is the intercept related to the diffusion boundary layer thickness. This model is based on film diffusion, intraparticles diffusion and final equilibrium stage. In some cases, the third region is absent [35].

The plot q_t versus $t^{1/2}$ is similar to Fig. 5. Two linear regions were observed. This reflects that more than one process affects the adsorption of dye onto the adsorbent. As the fitted lines do not pass through the origin, the intraparticle diffusion is not the only rate limiting mechanism.

The correlation coefficient and fitting parameters of this method are calculated and listed in Table 2.

The sharper region can be attributed to the rapid external diffusion and surface adsorption, and the second region is corresponding to the intraparticle diffusion [20,35–36].

3.2.2. Adsorption isotherm

To optimize the design of the sorption system, the informations on the capacity of the adsorbent, distribution of the dye molecules between the solid and liquid phases at the steady state and the nature of the dye and surface interactions are essential. The adsorption isotherm provides these qualitative informations. The adsorption isotherm of BB 41 onto NPS is presented in Fig. 7. Sharp increase of q_e at lower equilibrium solution concentration and then reaching a plateau shape at higher equilibrium solution concentration where the adsorption reached to the saturation form, demonstrates a high affinity between the dye molecules and hydroxyl groups on the adsorbent. In this study, Langmuir and Freundlich isotherms were used to describe the experimental data. The main assumption of Langmuir isotherm theory is the monolayer adsorption of adsorbate over the specific homogeneous sites within the adsorbent. The linearized Langmuir isotherm is expressed as follows:

$$\frac{C_e}{q_e} = \frac{1}{bq_m} + \frac{C_e}{q_m} \quad (5)$$

where C_e (mg/L) and q_e (mg/g) are the equilibrium adsorbate concentration in aqueous and solid phases, respectively and q_m is the maximum monolayer adsorption capacity. The values of q_m and b are determined from the linear plot of C_e/q_e versus C_e (Fig. 8).

A constant separation factor R_L is given by:

$$R_L = \frac{1}{1 + bC_0} \quad (6)$$

where b is the Langmuir coefficient and C_0 is the initial dye concentration. R_L indicates the favorability of the adsorption process. The adsorption process is a favorable ($0 < R_L < 1$), unfavorable ($R_L > 1$), linear ($R_L = 1$) and irreversible ($R_L = 0$). The value of R_L is consistent with the favorability of the adsorption process.

Table 2

Kinetic parameters of BB 41 adsorption onto NPS obtained using intraparticle diffusion model.

C_0 mg/L	$k_{i,1}$ mg/(g min ^{1/2})	C_1 mg/g	R^2	$k_{i,2}$ mg/(g min ^{1/2})	C_2 mg/g	R^2
20	4.5954	12.007	0.8929	0.2067	35.634	0.5313
40	12.042	16.208	0.9800	0.5261	69.63	0.9042
60	12.076	34.343	0.9899	0.8175	102.79	0.9031

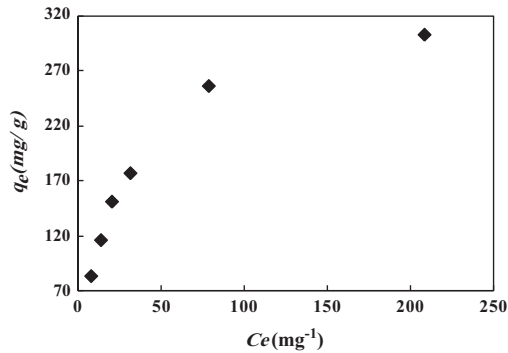


Fig. 7. Adsorption isotherm of BB 41 onto NPS.

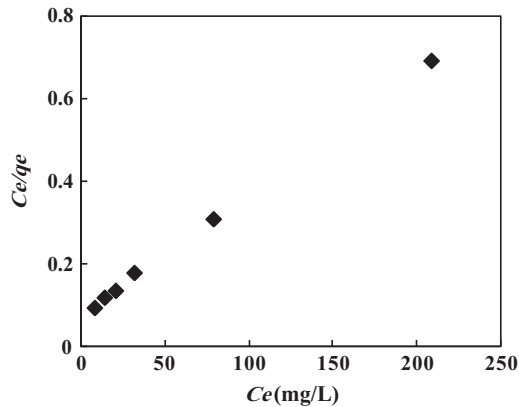


Fig. 8. Adsorption isotherm of BB 41 onto NPS using Langmuir model.

The Freundlich isotherm is assuming that the adsorption process is multilayer on the heterogeneous surface. This isotherm can be expressed as follows:

$$\log q_e = \log K_f + (1/n)\log C_e \quad (7)$$

where q_e and C_e are the adsorbate equilibrium concentrations in the solid and liquid phases, K_f and n denote Freundlich's uptake factor and intensity factor, respectively. The isotherm is favorable when $n > 1$, linear when $n = 1$ and unfavorable when $n < 1$.

The isotherm parameters are represented in Table 3. By contrasting R^2 values, it is found that the Langmuir model fitted better with experimental data than Freundlich model.

Table 3

Langmuir and Freundlich isotherms parameters for the adsorption of BB 41 onto NPS.

Langmuir model				K_f	Freundlich model	
q_m (mg/g)	b (L/mg)	R^2	R_L		n	R^2
345	0.04	0.9995	0.3–0.06	43	2.6	0.9533

Table 4

Comparison of the adsorption capacity of BB 41 onto various adsorbents.

Adsorbents	q_m (mg/g)	References
Sodium alginate	12	[32]
Untreated antibiotic waste	111	[33]
N, F-codoped flower-like TiO ₂	143	[31]
Montmorillonite	713	[36]
NPS	345	This work

The surface of silica has the negative charge at pH=7 due to silanolate groups and there are some hydroxyl group on the silica surface. The interaction of cationic dye molecules may be occurred via electrostatic interaction and hydrogen bonding.

In comparison with the adsorption capacities of other adsorbents (Table 4), the adsorption capacity of NPS was found to be better than the most other adsorbents reported in the literature [31–33,37]. The higher capacity of montmorillonite is due to the adsorption and H-aggregates of the dye on the clays.

4. Conclusion

In summery, NPS with an average pore diameter of 2.4 nm and a surface area of 1030 m²/g was synthesized by using NP-10 and ETS-40 under acidic condition. The adsorption of BB 41 from aqueous solution with NPS was investigated by looking into equilibrium and kinetics aspects. The adsorption kinetic studies revealed that the adsorption process followed the pseudo-second-order model. The adsorption pattern of BB 41 onto NPS was well fitted with Langmuir isotherm model. The monolayer adsorption capacity of BB 41 onto NPS was found to be 345 mg/g which is better than most of the other adsorbents. This study indicated that NPS could be used as a potential adsorbent for the removal of cationic dye in wastewaters.

Acknowledgment

We would like to express our gratitude to the University of Tehran for support of this work.

References

- [1] B.E. Reed, M.R. Matsumoto, J.N. Jensen, R. Viadero Jr., W. Lin, Physicochemical processes, *Water Environ. Res.* 70 (1998) 449–473.
- [2] H.M. Pinheiro, E. Touraud, O. Thomas, Aromatic amines from azo dye reduction: status review with emphasis on direct UV spectrophotometric detection in textile industry wastewaters, *Dyes Pigments* 61 (2004) 121–139.
- [3] J. Griffiths, Developments in the light absorption properties of dyes—color and photochemical reactions, in: J. Griffiths (Ed.), *Developments in the Chemistry and Technology of Organic Dyes*, Society of Chemistry Industry, Oxford 1984, pp. 1–30.
- [4] K. Dutta, S. Mukhopadhyay, S. Bhattacharjee, B. Chaudhuri, Chemical oxidation of methylene blue using a Fenton-like reaction, *J. Hazard. Mater.* 84 (2001) 57–71.
- [5] M. Kornaros, G. Lyberatos, Biological treatment of wastewaters from a dye manufacturing company using a trickling filter, *J. Hazard. Mater.* 136 (2006) 95–102.

- [6] J.-W. Lee, S.-P. Choi, R. Thiruvenkatachari, W.-G. Shim, H. Moon, Submerged microfiltration membrane coupled with alum coagulation/powdered activated carbon adsorption for complete decolorization of reactive dyes, *Water Res.* 40 (2006) 435–444.
- [7] C.-H. Liu, J.-S. Wu, H.-C. Chiu, S.-Y. Suen, K.H. Chu, Removal of anionic reactive dyes from water using anion exchange membranes as adsorbents, *Water Res.* 41 (2007) 1491–1500.
- [8] M. Muruganandham, M. Swaminathan, TiO₂-UV photocatalytic oxidation of Reactive Yellow 14: effect of operational parameters, *J. Hazard. Mater.* 135 (2006) 78–86.
- [9] Z. Yan, S. Tao, J. Yin, G. Li, Mesoporous silicas functionalized with a high density of carboxylate groups as efficient adsorbents for the removal of basic dyestuffs, *J. Mater. Chem.* 16 (2006) 2347–2353.
- [10] Y.C. Pei, J.J. Wang, X.P. Xuan, J. Fan, M. Fan, Factors affecting ionic liquids based removal of anionic dyes from water, *Environ. Sci. Technol.* 41 (2007) 5090–5095.
- [11] R.S. Blackburn, Natural polysaccharides and their interactions with dye molecules: applications in effluent treatment, *Environ. Sci. Technol.* 38 (2004) 4905–4909.
- [12] S.S. Vaghela, A.D. Jethva, B.B. Mehta, S.P. Dave, S. Adimurthy, G. Ramachandriah, Laboratory studies of electrochemical treatment of industrial Azo dye effluent, *Environ. Sci. Technol.* 39 (2005) 2848–2855.
- [13] E. Mitter, G. Santos, É. Almeida, L. Morão, H. Rodrigues, C. Corso, Analysis of acid Alizarin Violet N dye removal using sugarcane bagasse as adsorbent, *Water Air Soil Pollut.* 223 (2012) 765–770.
- [14] M. Akgül, A. Karabakan, Promoted dye adsorption performance over desilicated natural zeolite, *Microporous Mesoporous Mater.* 145 (2011) 157–164.
- [15] F. Liu, S. Chung, G. Oh, T.S. Seo, Three-dimensional graphene oxide nanostructure for fast and efficient water-soluble dye removal, *ACS Appl. Mater. Interfaces* 4 (2011) 922–927.
- [16] L. Wang, J. Zhang, R. Zhao, C. Li, Y. Li, C. Zhang, Adsorption of basic dyes on activated carbon prepared from *Polygonum orientale* Linn: equilibrium, kinetic and thermodynamic studies, *Desalination* 254 (2010) 68–74.
- [17] Y. Wang, W. Chu, Adsorption and removal of a xanthene dye from aqueous solution using two solid wastes as adsorbents, *Ind. Eng. Chem. Res.* 50 (2011) 8734–8741.
- [18] K.Y. Ho, G. McKay, K.L. Yeung, Selective adsorbents from ordered mesoporous silica, *Langmuir* 19 (2003) 3019–3024.
- [19] C.-H. Huang, K.-P. Chang, H.-D. Ou, Y.-C. Chiang, C.-F. Wang, Adsorption of cationic dyes onto mesoporous silica, *Microporous Mesoporous Mater.* 141 (2011) 102–109.
- [20] F. Liu, J. Wang, L. Li, Y. Shao, Z. Xu, S. Zheng, Adsorption of Direct Yellow 12 onto ordered mesoporous carbon and activated carbon, *J. Chem. Eng. Data* 54 (2009) 3043–3050.
- [21] A.R. Cestari, E.F.S. Vieira, G.S. Vieira, L.P. da Costa, A.M.G. Tavares, W. Loh, C. Airoldi, The removal of reactive dyes from aqueous solutions using chemically modified mesoporous silica in the presence of anionic surfactant—The temperature dependence and a thermodynamic multivariate analysis, *J. Hazard. Mater.* 161 (2009) 307–316.
- [22] J.B. Joo, J. Park, J. Yi, Preparation of polyelectrolyte-functionalized mesoporous silicas for the selective adsorption of anionic dye in an aqueous solution, *J. Hazard. Mater.* 168 (2009) 102–107.
- [23] H. Yang, Q. Feng, Characterization of pore-expanded amino-functionalized mesoporous silicas directly synthesized with dimethyldecylamine and its application for decolorization of sulphonated azo dyes, *J. Hazard. Mater.* 180 (2010) 106–114.
- [24] S. Jain, R.V. Jayaram, Removal of basic dyes from aqueous solution by low-cost adsorbent: wood apple shell (*Feronia acidissima*), *Desalination* 250 (2010) 921–927.
- [25] X. Fu, X. Chen, J. Wang, J. Liu, Fabrication of carboxylic functionalized superparamagnetic mesoporous silica microspheres and their application for removal basic dye pollutants from water, *Microporous Mesoporous Mater.* 139 (2011) 8–15.
- [26] S. Wang, H. Li, L. Xu, Application of zeolite MCM-22 for basic dye removal from wastewater, *J. Colloid Interface Sci.* 295 (2006) 71–78.
- [27] X.S. Wang, Y. Zhou, Y. Jiang, C. Sun, The removal of basic dyes from aqueous solutions using agricultural by-products, *J. Hazard. Mater.* 157 (2008) 374–385.
- [28] Y.H. Chen, Synthesis, characterization and dye adsorption of ilmenite nanoparticles, *Journal of Non-Cryst. Solids* 357 (2011) 136–139.
- [29] Y. Zhang, S. Xu, Y. Luo, S. Pan, H. Ding, G. Li, Synthesis of mesoporous carbon capsules encapsulated with magnetite nanoparticles and their application in wastewater treatment, *J. Mater. Chem.* 21 (2011) 3664–3671.
- [30] A.Z.M. Badruddoza, G.S.S. Hazel, K. Hidajat, M.S. Uddin, Synthesis of carboxymethyl- β -cyclodextrin conjugated magnetic nano-adsorbent for removal of methylene blue, *Colloids Surf. A: Physicochem. Eng. Asp.* 367 (2010) 85–95.
- [31] Y. Jiang, Y. Luo, F. Zhang, L. Guo, L. Ni, Equilibrium and kinetic studies of C.I. Basic blue 41 adsorption onto N, F-codoped flower-like TiO₂ microspheres, *Appl. Surf. Sci.* 273 (2013) 448–456.
- [32] N.M. Mahmoodi, B. Hayati, M. Arami, Kinetic, equilibrium and thermodynamic studies of ternary system dye removal using a biopolymer, *Ind. Crops Prod.* 35 (2012) 295–301.
- [33] N. Yeddou-Mezenner, Kinetics and mechanism of dye biosorption onto an untreated antibiotic waste, *Desalination* 262 (2010) 251–259.
- [34] M. Zarezadeh-Mehrizi, A. Badii, A.R. Mehrabadi, Ionic liquid functionalized nanoporous silica for removal of anionic dye, *J. Mol. Liq.* 180 (2013) 95–100.
- [35] B.H. Hameed, Spent tea leaves: a new non-conventional and low-cost adsorbent for removal of basic dye from aqueous solutions, *J. Hazard. Mater.* 161 (2009) 753–759.
- [36] L. Ai, C. Zhang, L. Meng, Adsorption of Methyl Orange from aqueous solution on hydrothermal synthesized Mg–Al layered double hydroxide, *J. Chem. Eng. Data* 56 (2011) 4217–4225.
- [37] M. Roulia, A.A. Vassiliadis, Sorption characterization of a cationic dye retained by clays and perlite, *Microporous Mesoporous Mater.* 116 (2008) 732–740.